This is a non-peer reviewed technical note submitted to EarthArXiv to supplement the article *A multi-GNSS, multi-frequency and near real-time ionospheric TEC monitoring system for South America*, by Mendoza, L. P. O., Meza, A. M. and Aragón Paz, J. M. (2019), in Space Weather (in preparation) .....

Technical note on the multi-GNSS, multi-frequency and near real-time ionospheric TEC monitoring system for South America

Mendoza, L. P. O. and Meza, A. M. and Aragón Paz, J. M.
Laboratorio de Meteorología espacial, Atmósfera terrestre, Geodesia, Geodinámica, diseño de Instrumental y Astrometría (MAGGIA), Facultad de Ciencias Astronómicas y Geofísicas (FCAG), Universidad Nacional de La Plata (UNLP), Paseo del Bosque s/n, B1900FWA, La Plata, Argentina
and
Consejo Nacional de Investigaciones Científicas y Técnicas (CONICET), Godoy Cruz 2290, C1425FQB, Buenos Aires, Argentina
web: www.maggia.unlp.edu.ar
e-mail: lmendoza@fcaglp.unlp.edu.ar (first author)

in: EarthArXiv. See also BibTeX entry below.

BibTeX:

```
@article{tn,
  author      = {Mendoza, L. P. O. and Meza, A. M. and {Aragón Paz}, J. M.},
  title       = {Technical note on the multi-GNSS, multi-frequency and near real-time
                 ionospheric TEC monitoring system for South America},
  journal     = {EarthArXiv},
  pages       = {1--11},
  year        = {2019},
  doi         = {not yet assigned}
}
```


document created on: February 21, 2019
created from file: tn.tex
cover page automatically created with CoverPage.sty
(available at your favourite CTAN mirror)

MAGGIA LABORATORIO

UNIVERSIDAD NACIONAL DE LA PLATA

CONICET

Technical note on the multi-GNSS, multi-frequency and near real-time ionospheric TEC monitoring system for South America

Luciano. P. O. Mendoza[1,2], Amalia M. Meza[1,2], and Juan Manuel Aragón Paz[1,2]

[1]Laboratorio de Meteorología espacial, Atmósfera terrestre, Geodesia, Geodinámica, diseño de Instrumental y Astrometría (MAGGIA), Facultad de Ciencias Astronómicas y Geofísicas (FCAG), Universidad Nacional de La Plata (UNLP), Paseo del Bosque s/n, B1900FWA, La Plata, Argentina
[2]Consejo Nacional de Investigaciones Científicas y Técnicas (CONICET), Godoy Cruz 2290, C1425FQB, Buenos Aires, Argentina

February 21, 2019

Abstract

Development of regional services able to provide ionospheric total electron content (TEC) maps with a high spatial resolution, and in near real-time, are of high importance for applications and the research community. We provide here the methodologies, and a preliminary assessment, of such a system. The system relies on the public Global Navigational Satellite Systems (GNSS) infrastructure in South America, it incorporates data from multiple constellations (currently GPS, GLONASS, Galileo and BeiDou), it employs multiple frequencies, and it produces continental-wide TEC maps with a latency of just few minutes. A year-round comparison of the produced maps with several products issued by the International GNSS Service (IGS) resulted in mean biases lower than 1 TEC units (TECU), whereas their evaluation against direct and independent GNSS-based slant TEC measurements resulted in accuracies of the same magnitude.

1 System Description

1.1 Real-time Data

Regional GNSS observations are continuously acquired, by means of the *BNC* software (Weber et al., 2016), from streams broadcasted by several agencies: the Bundesamt für Kartographie und Geodäsie (BKG, Germany) and the National Aeronautics and Space Administration (NASA, USA), both in support to the IGS, by the Instituto Brasileiro de Geografia e Estatística (IBGE, Brazil), by the Instituto Geográfico Nacional (IGN, Argentina), by the Servicio Geográfico Militar (SGM, Uruguay) and by UNAVCO (USA) (see Table 1). In total, observations from more than two hundred ground stations, mostly located in South America but also from Central and North America, Europe, Africa and Antarctica, are employed by the TEC monitoring system. In addition, GPS, GLONASS, Galileo and BeiDou broadcasted orbit and clock messages, disseminated by the IGS Real-Time Service (IGS-RTS, Rülke et al., 2014), are employed. This stream is also provided by BKG. Once locally stored the data set is managed with the help of the *gfzrnx* software tool (Nischan, 2016), particularly useful for the concatenation of multiple RINEX files (Gurtner and Estey, 2017). The monitoring system exclusively relies on the availability of these data streams, and no additional products are required.

1.2 Data Preprocessing

Before any computation a per station preprocessing and data cleaning is performed. This includes the application of an appropriate time window, of an elevation cut off angle, of carrier phase wind-up corrections and the determination of phase-continuous intervals (i.e., with constant ambiguity). The data cleaning is non-parametric and consists in three steps. Firstly, pairs of satellite-receiver phase and code links, in two bands, are optimally selected according to the amount of available observations and the tracking modes, or channel attribute, employing the same default priorities as the ones defined by

Table 1: Data sources employed by the near real-time ionospheric TEC monitoring system for South America.

Organization	Real-time streams at[†]

Bundesamt für Kartographie und Geodäsie (Germany)	`http://products.igs-ip.net`
	`http://www.igs-ip.net`
	`http://mgex.igs-ip.net`

Instituto Brasileiro de Geografia e Estatística (Brazil)	`http://170.84.40.52`
Instituto Geográfico Nacional (Argentina)	`http://ntrip.ign.gob.ar`
National Aeronautics and Space Administration (USA)	`https://cddis-caster.gsfc.nasa.gov`
Servicio Geográfico Militar (Uruguay)	`http://rtk.sgm.gub.uy`
UNAVCO (USA)	`http://rtgpsout.unavco.org`

[†]Registration may be required in order to access same of the data streams.

Nischan (2016). The corresponding, undifferenced, Melbourne-Wübbena (MW) linear combinations are screened for outliers and cycle slips (Table 2). Any possible receiver's clock inconsistency between phase and code observations is handled as a cycle slip. Secondly, a per band, time-differenced, phase screening is performed, for unnoticed outliers and cycle slips. These screenings, performed both for- and backward in time, are repeated until no additional cycle slips, or outliers, are found. Furthermore, no attempt is made to correct any cycle slip. Finally, MW and (cuasi) ionosphere-free (IF) linear combinations, within each phase-continuous interval, are formed and modeled with low degree polynomials. Intervals resulting in residuals with root mean squared (RMS) greater than given thresholds are rejected. In total, less than 7 % of the original observations are generally left out, including those observations bellow the elevation cut off angle.

Thereafter, a clean and single set of undifferenced carrier phase $\phi_{ij,k}$ (in cycles), code pseudorange $C_{ij,k}$ (in meters) and signal-to-noise ratio $\mathrm{SN}_{ij,k}$ observables, between each pair of satellite i and receiver j, and for each tracked band k, is obtained. This data preprocessing is performed with the Fortran 2008 + OpenMP, in-house developed, software *AGEO* (library for Geodetic and Orbital Analysis or *biblioteca de Análisis GEodésico y Orbital*, in Spanish). In addition, it is externally parallelized, on a per station basis, by means of the *GNU parallel* software tool (Tange, 2011).

Table 2: Pairs of bands employed in the Melbourne-Wübbena (MW) data screening, with their corresponding wide-lane wavelengths λ_{WL} (in meters). Those pairs of bands employed in the computation of geometry-free (GF) linear combinations and inter-frequency biases (IFBs) are also indicated. Observation codes according to RINEX version 3.03 (Gurtner and Estey, 2017).

GNSS	Bands		λ_{WL}	GF & IFB
GPS	L2	L5	5.86	no
	L1	L2	0.86	yes
	L1	L5	0.75	yes
GLONASS	L2	L3	6.82	no
	L1	L2	0.84	yes
	L1	L3	0.75	yes
Galileo	L7	L5	9.77	no
	L7	L6	4.19	no
	L6	L8	3.54	no
	L6	L5	2.93	no
	L1	L6	1.01	yes
	L1	L7	0.81	yes
	L1	L8	0.78	yes
	L1	L5	0.75	yes
BeiDou	L6	L7	4.88	no
	L2	L6	1.04	yes
	L2	L7	0.84	yes

1.3 Hardware Delays Calibration

Once per hour inter-frequency biases (IFBs) are estimated from carrier-to-code leveled geometry-free (GF) linear combinations (see, e.g., Spits, 2012). These hardware delays are solved simultaneously with spherical harmonic (SH) coefficients of a single-layer VTEC representation (Schaer, 1999), assuming that all free electrons are constrained to an infinitesimally thin layer at a height of 450 km. Here only independent linear combinations are employed, between selected pairs of bands (Table 2). Hence, only independent IFBs are computed. Also, no closing restriction is imposed, resulting in satellite-receiver-, pair-of-bands-specific IFBs. Moreover, different tracking modes or channel attributes, between each pair of satellite-receiver links, are taken into account. The estimation is made by means of a weighted least squares adjustment, performed also with the *AGEO* software, and executed in one single step, involving the most recent observations available, from all ground stations and all satellites, within the previews 24 hours (i.e., a 24 hours rolling- or moving-window).

In practice, after preprocessing the raw observations corresponding to each pair satellite i and receiver j, and for each pair of bands k and l, all possible carrier-to-code leveled GF linear combinations $\widetilde{L}_{\mathrm{GF},ij,kl}$ (in meters) are computed by

$$\widetilde{L}_{\mathrm{GF},ij,kl} = L_{\mathrm{GF},ij,kl} - \langle L_{\mathrm{GF},ij,kl} - C_{\mathrm{GF},ij,kl} \rangle \tag{1}$$

where $L_{\mathrm{GF},ij,kl} = \lambda_k \phi_{ij,k} - \lambda_l \phi_{ij,l}$ are the non-leveled GF linear combinations in phase (in meters) and $C_{\mathrm{GF},ij,kl} = C_{ij,l} - C_{ij,k}$ are the corresponding linear combinations in code pseudorange (in meters), being λ_k and λ_l the wavelengths of each band (in meters). Here the average is computed within each phase-continuous interval, under the assumption of stable hardware delays. This commonly used methodology reduces the observations noise, from code to phase levels, and avoids the estimation of phase ambiguities, but it could also introduce some systematic errors (see, e.g., Ciraolo et al., 2007; Spits, 2012). In addition, each GF observation is weighted according to three factors: the instantaneous satellite elevation, the amount of observations employed during the carrier-to-code leveling (i.e., the lenght of each phase-continuous interval) and the corresponding navigational system (GPS, GLONASS, Galileo or BeiDou, see Ren et al., 2016). Then, the full set of GF observations is represented as

$$\widetilde{L}_{\mathrm{GF},ij,kl} = \alpha_{kl}\, \mathrm{MF}(z)\, \mathrm{VTEC}(\mu, t) + \mathrm{IFB}_{ij,kl} \tag{2}$$

where $\mathrm{MF}(z)$ is the Modified Single Layer Model (MSLM) mapping function (Schaer, 1999), being z the zenith distance of satellite i as seen by receiver j (in radians), $\mathrm{IFB}_{ij,kl}$ are the corresponding specific IFBs (in meters), α_{kl} is a proportionality constant (in meters per TECU, where 1 TECU is equivalent to 10^{16} free e^- per squared meter)

$$\alpha_{kl} = 40.3 \times 10^{16} \left(\frac{1}{f_k^2} - \frac{1}{f_l^2} \right) \tag{3}$$

being f_k and f_l the frequencies of each band (in Hertz), whereas the VTEC is expressed as a SH expansion in a sun-fixed frame

$$\mathrm{VTEC}(\mu, t) = \sum_{n=0}^{n_{\max}} \sum_{m=0}^{n} \overline{P}_{nm}(\sin \mu) \big(a_{nm} \cos(m\, t) + b_{nm} \sin(m\, t) \big). \tag{4}$$

Here a_{nm} and b_{nm} are the coefficients of the SH expansion (in TECU), with maximum degree n_{max}, whereas $\overline{P}_{nm}$ are the corresponding Real Associated Legendre Functions (4π normalized, see for example Wieczorek and Meschede, 2018), t is the Local Time (LT, in radians) and μ is the modified dip latitude (also in radians). In this case the algorithms issued by the European GNSS (Galileo) Open Service (2016), together with the corresponding global grid, are employed for the computation of μ.

As only regional observations are employed, the 24 hours time window helps into decoupling the hardware delays, from the ionospheric parameters, by always including in the adjustment observations spanning 24 hours of LT. Furthermore, a single set of constant coefficients a_{nm} and b_{nm}, loosely constrained to a *zero* ionosphere, is estimated for the entire time span, resulting in a mean (daily) VTEC representation. For the same reason a SH expansion of low degree is employed, in order to avoid ill conditioned normal equations (Haines, 1985), which in turn could produce mapping artifacts, particularly at the boundaries of the region. On the other hand, the $\mathrm{IFB}_{ij,kl}$ are also parametrized as constants, and estimates with mean observational epoch at the middle of each moving-window are obtained. These hardware delays are also loosely constrained to their most recently estimated values. In fact, the main result of this hourly adjustment are precisely these decoupled $\mathrm{IFB}_{ij,kl}$ estimates. However, they result systematically half a day old.

1.4 Near Real-Time TEC Mapping

Every 15 minutes, and also by means of a weighted least squares adjustment, both the IFBs and the SH coefficients for the regional VTEC representation are updated. In essence, the same software, methodology and parametrization described in the previews section are employed. However, in this case only the most recent observations available, within a one hour moving-window, are used. In addition, here four sets of pice-wise constant SH coefficients are estimated, each one valid for a quarter of an hour. Furthermore, the $\mathrm{IFB}_{ij,kl}$ parameters are now actively constrained to their most recent, hourly, and decoupled estimates. In practice, this results in new hardware delays estimates that are simultaneously up-to-date (i.e., less than 30 minutes old) and decoupled from the coefficients of the SH expansion. Thereafter, tracks of instantaneous, VTEC estimates are obtained from the original GF observations by

$$\mathrm{VTEC}_{ij,kl,\varphi\lambda} = \big(\alpha_{kl}\,\mathrm{MF}(z)\big)^{-1}\big(\widetilde{L}_{\mathrm{GF},ij,kl} - \mathrm{IFB}_{ij,kl}\big) \tag{5}$$

where φ and λ are the geographic latitude and longitude, respectively, of the ionospheric pierce points (IPPs), that is, the intersection point between the instantaneous satellite-receiver line-of-sight with the single layer of the model. Similarly, traces of slant TEC (STEC) estimates can be computed by

$$\mathrm{STEC}_{ij,kl,\varphi\lambda} = \alpha_{kl}^{-1}\big(\widetilde{L}_{\mathrm{GF},ij,kl} - \mathrm{IFB}_{ij,kl}\big). \tag{6}$$

At this point two representations of the current state of the regional ionospheric TEC are available. In one hand, an analytical representation, given by the coefficients of a low degree SH expansion in μ and t, with mean epoch at the middle of the latest 15 minutes of the observational window. On the other hand, a discreet and huge set of instantaneous $\mathrm{VTEC}_{ij,kl,\varphi\lambda}$ estimates, along the IPP tracks, during the same interval. In fact, the issued TEC product is obtained by mapping these tracks in the space domain.

This postprocessing of the $\mathrm{VTEC}_{ij,kl,\varphi\lambda}$ estimates comprises three steps, all performed with the *Generic Mapping Tools* software package (GMT, Wessel et al., 2013). Firstly, all available estimates are averaged within the cells of a uniform 0.5×0.5 degrees grid, previously discarding cells with very few observations, and effectively resulting in N space- and time-averaged $\langle\mathrm{VTEC}\rangle_p$ values, for $p = 1, \ldots, N$. Secondly, this regular grid is approximated, using a generalized Green's function for continuous curvature spherical spline in tension (Wessel and Becker, 2008), by

$$\mathrm{VTEC}(\varphi,\lambda) = c_0 + \sum_{p=1}^{M} c_p\, g(\varphi,\lambda,\varphi_p,\lambda_p) \tag{7}$$

where φ and λ are arbitrary coordinates, $M \leq N$ is the number of employed coefficients, φ_p and λ_p are the coordinates of the corresponding cells, c_0 is the mean VTEC over all populated cells (in TECU), g is the generalized Green's function and c_p are the spline coefficients (also in TECU), solved for by Singular-Value Decomposition (SVD) on the square linear system

$$\langle\mathrm{VTEC}\rangle_p - c_0 = \sum_{q=1}^{N} c_q\, g(\varphi_p,\lambda_p,\varphi_q,\lambda_q) \tag{8}$$

and retaining only those M eigenvalues whose ratios, to the largest, are greater than a given threshold. While we empirically determined optimal (fixed) values for both the tension and the threshold, searching over thousand of maps for minimization of the misfits, the number M of contributing eigenvalues is dynamically determined, every time, to accommodate the variance of the current data. That is, the more spatial variability in the regional VTEC the more eingenvalues are retained in the mapping procedure. Finally, the adjusted function is evaluated on a uniform 0.5×0.5 degrees grid and areas far away from IPP tracks are automatically masked out. The resulting grid constitutes the actual, near real-time, regional TEC map produced by the system, as no additional postprocessing (e.g., smoothing) is required nor performed.

2 System Assesment

2.1 Year-round Intercomparison with Global Products

To evaluate the quality of the produced maps, and particularly the possible presence of systematic biases, we compared them with several IGS final TEC products, provided in IONEX format, and computed by

several IGS Ionosphere Associated Analysis Centers (IAACs): Center for Orbit Determination in Europe (CODE, Switzerland; see Schaer, 1999), European Space Agency/European Space Operations Centre (ESA/ESOC, Germany, see Feltens, 2007), IGS (see Hernández-Pajares et al., 2009), Jet Propulsion Laboratory/National Aeronautics and Space Administration (JPL/NASA, USA; see Mannucci et al., 1998) and Universitat Politècnica de Catalunya (UPC, Spain; see Hernández-Pajares et al., 1999; Orús et al., 2005). From UPC we employed both, their standard and their high rate products. We also included in the analysis TEC products from two additional IGS ACs: Natural Resources Canada (NRCAN, Canada; see Ghoddousi-Fard et al., 2011) and Wuhan University (WHU, China; see Wang et al., 2018). These products are usually available with latencies of a few days or, at best, several hours. In addition, we also included in the intercomparison the (non-IGS) global and high resolution TEC products provided by the Massachusetts Institute of Technology (MIT Haystack Observatory, USA; see Rideout and Coster, 2006). All IGS maps were retrieved from `ftp://cddis.gsfc.nasa.gov/gnss/products/ionex/`. The maps from MIT were retrieved from `http://millstonehill.haystack.mit.edu/`.

The comparison extends a full year, from June 1, 2017 to May 31, 2018, and it was performed on a map by map basis (i.e., epoch by epoch). In order to assess the expected differences we performed the same one-to-one comparison between pairs of global products. Although these maps have global coverage, the comparison was restricted to the area covered by our regional maps, that is, between 80° S and 40° N in latitude and 110° W and 0° E in longitude (see Figure 1 in Mendoza et al., 2019). Also, no spatial or temporal interpolation was performed. Rather, only TEC samples at common epochs, and exactly the same reported locations, were differenced. For this reason, and before the comparisons, our high resolution maps were downsampled. Thus, the results were controlled by the standard 5×2.5 degrees spatial sampling (in longitude and latitude, respectively) of the IGS products or, alternatively, by the 1×1 degrees spatial sampling of the MIT products.

For this analysis, instead of the real-time data streams, we employed daily observational and navigational RINEX files available at the servers of the respective data providers. However, to reproduce exactly the results of the near real-time system, we only used data from those GNSS stations that are actually accessible in real-time, leaving all off-line stations out of the analysis. We also employed the very same broadcasted orbits and satellite clocks, and no other products. In addition, we followed exactly the same two-steps methodology previously described. That is, a first step resulted in IFBs estimates, from a 24 hours observational moving-window, while in a second and final step the TEC maps were produced, from a 15 minutes moving-window. To speed up this year-round analysis, and although some of the selected products are currently provided at a higher rate (e.g.,by CODE, NRCAN and particularly UPC and MIT), we computed maps with 2 hours of temporal sampling, following the classical IGS standard practice.

The year-round (and regional) comparison shows the existence of systematic differences between all the analyzed pairs of TEC products (Table 3). In average, our near real-time TEC maps show a very good agreement with the maps produced by ESA/ESOC, CODE, UPC (high rate) and especially NRCAN, resulting for all the cases in a mean bias lower or equivalent to 1 TECU, comparable with the differences found between pairs of global products. Nevertheless, while there seems to be no significantly biases between both, our products and the ones from NRCAN and between them and the ones from CODE, a small systematic bias do exists between the former and our products. The reason for this seemingly discordant results is simple: given their global coverage, the comparisons between pairs of IGS products span the entire area mapped (Figure 1 in Mendoza et al., 2019), whereas those comparisons involving our regional product are mostly restricted to the land, leaving large portions of the oceans out of the analysis, and this is evident in the lower number of common TEC samples found (Table 3). This contributes also to the higher mean standard deviation encountered while comparing our maps with the other products, both in average and individually (Figure 1). Indeed, not only a smaller number of differences are averaged, also the smoothest areas of the IGS maps over the oceans, where no actual GNSS observations were available, are systematically left out of these comparisons. At the same time, all comparisons show, to a greater or lesser extent, smaller variance during the southern winter (i.e., June, July and August). This is probably due to the lower, regional, mean ionospheric TEC in that season.

2.2 Differential STEC Evaluation

In order to independently assess the accuracy of the produced TEC maps we applied a differential STEC (dSTEC) test developed by the IGS Ionosphere Working Group (IIWG) for the evaluation, and relative weighting, of their Global Ionosphere Maps (GIMs) (see, for example, Orús et al., 2007, 2005; Roma-Dollase et al., 2018). In essence, the test is based on the ability to make highly accurate dSTEC

Table 3: Year-round one-to-one comparison between selected (GNSS based) TEC products, from June 1, 2017 to May 31, 2018: codg (CODE), emrg (NRCAN), esag (ESA/ESOC), igsg (IGS, combination of codg and jplg), jplg (JPL/NASA), mapgps (MIT), upcg (UPC), uqrg (UPC, high rate), whug (WHU) and magn (our near real-time product). The mean difference $\overline{x}_{A-B}$ and mean standard deviation $\overline{\sigma}_{A-B}$, over all compared maps, are expressed in TECU.

Products				TEC	TEC
A	B	$\overline{x}_{A-B}$	$\overline{\sigma}_{A-B}$	Maps	Samples
codg	magn	0.7	1.9	4380	1965432
	emrg	0.1	2.1	8758	9869733
	esag	−0.1	1.6	4368	4922736
	igsg	−1.0	0.6	4380	4936260
	jplg	−2.2	1.3	4380	4936260
	mapgps	2.3	2.3	8568	1232740
	upcg	−0.7	1.5	4284	4828068
	uqrg	−0.7	1.7	8736	9845472
	whug	1.7	4.4	5280	5950560
emrg	magn	0.1	2.4	4380	1965367
	esag	−0.2	2.6	4368	4922471
	igsg	−1.0	2.1	4380	4935994
	jplg	−2.2	2.4	4380	4935994
	mapgps	2.1	2.2	8566	1232401
	upcg	−0.8	2.0	4284	4827806
	uqrg	−0.7	2.3	8734	9842685
	whug	1.7	4.6	5278	5947974
esag	magn	0.9	2.2	4368	1960492
	igsg	−0.8	1.7	4368	4922736
	jplg	−2.0	2.0	4368	4922736
	mapgps	2.4	2.8	4272	614605
	upcg	−0.5	1.7	4272	4814544
	uqrg	−0.5	2.3	4356	4909212
	whug	2.4	5.0	4368	4922736
igsg	magn	1.6	1.9	4380	1965432
	jplg	−1.2	0.7	4380	4936260
	mapgps	3.3	2.3	4284	616229
	upcg	0.3	1.5	4284	4828068
	uqrg	0.3	1.6	4368	4922736
	whug	3.2	5.1	4380	4936260
jplg	magn	2.9	2.1	4380	1965432
	mapgps	4.6	2.4	4284	616229
	upcg	1.5	1.8	4284	4828068
	uqrg	1.5	1.8	4368	4922736
	whug	4.4	5.3	4380	4936260
mapgps	magn	−2.0	2.8	4284	10182540
	upcg	−2.7	2.3	4188	603294
	uqrg	−2.7	2.2	33470	4816557
	whug	−0.1	4.2	5160	749695
upcg	magn	1.1	1.9	4128	1848581
	uqrg	0.0	1.1	4272	4814544
	whug	2.9	4.9	4284	4828068
uqrg	magn	1.0	1.9	4369	1960667
	whug	2.3	4.7	5268	5937036
whug	magn	−2.7	5.0	4377	1963993

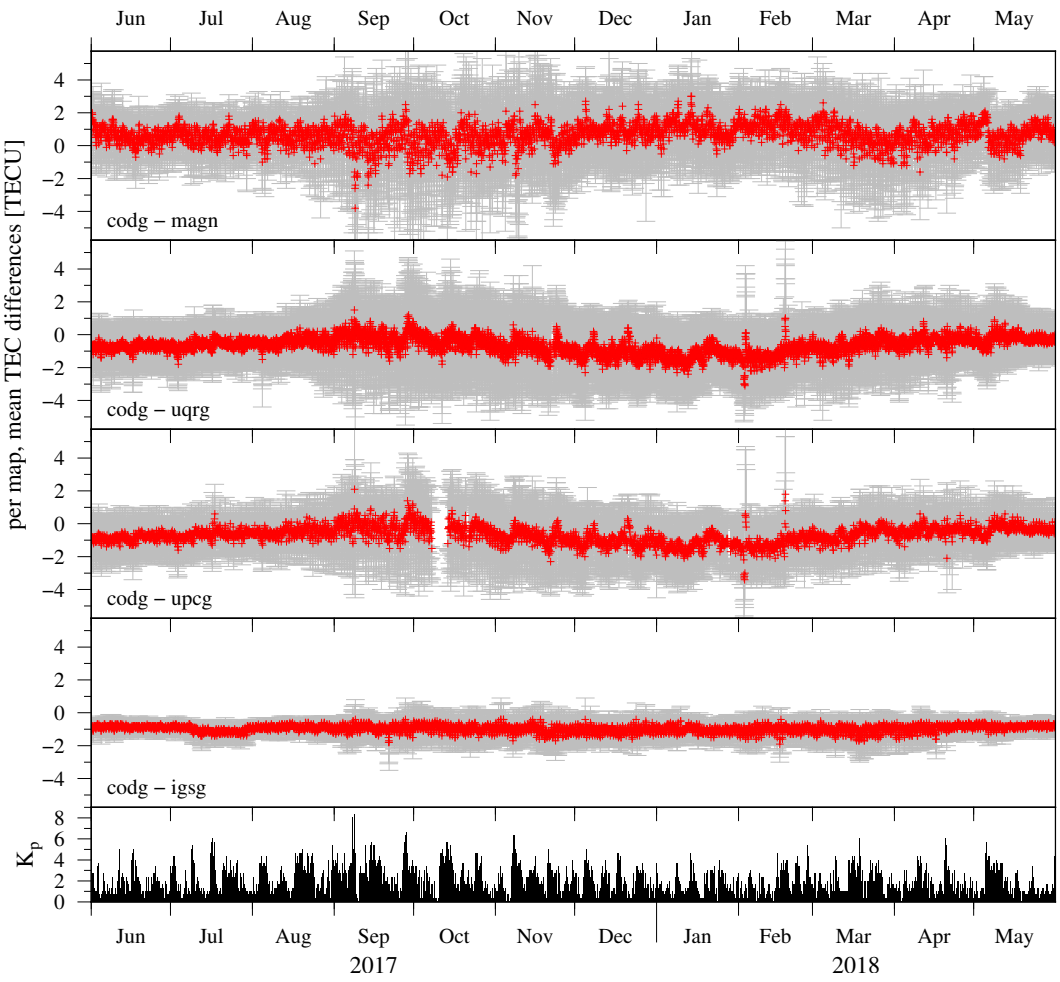

Figure 1: Examples of mean differences and standard deviations, per map, resulting from the year-round one-to-one TEC products comparisons: between a final IGS and our near real-time product (codg and magn, respectively), between two final IGS products (codg and the high rate uqrg), between two final IGS products (codg and upcg, noting that no upcg IONEX files were available for October 8–13 and 21, 2017 and for January 28, 2018) and between a final and the combined IGS product (codg and igsg, respectively). The global K_p index, provided by the GeoForschungsZentrum (GFZ, Germany), is also plotted.

measurements, on the order of 10^{-2} TECU (Coster et al., 2013; Hernández-Pajares et al., 2017), and to compare them with synthetic (i.e., mapped) dSTEC values. In fact, we employed the very same implementation of the test as described in detail by Hernández-Pajares et al. (2017), the only difference being our extension of the test to the multi-frequency case.

The analysis is performed on a per station basis, involving only GNSS stations that were not employed for the computation of the TEC maps being evaluated. Firstly, and after preprocessing the corresponding raw data (e.g., outliers rejection, phase wind-up correction, etc.), observed dSTEC_o (in TECU) are obtained from (non-leveled) carrier phase GF linear combinations (in meters) by

$$\mathrm{dSTEC}_o(t_s) = \alpha_{kl}^{-1}\left(L_{\mathrm{GF},ij,kl}(t_s) - L_{\mathrm{GF},ij,kl}(t_r)\right) \quad \text{with } t_r \neq t_s, \tag{9}$$

taking advantage of the total cancellation of the phase ambiguities within each phase-continuous interval. Here t_r (in hours) represents a reference epoch, when the satellite reaches its minimum zenith distance within each phase-continuous interval, whereas t_s (in hours) are all other sample epochs within the same phase interval. Here we employed a sampling rate of 60 seconds and, following the convention stated by Hernández-Pajares et al. (2017), only GF observations no more than 900 seconds apart were differenced. This results in a maximum of 30 dSTEC_o samples per phase-continuous interval, regardless of its total length. In addition, the corresponding zenith distances z_r and z_s (both in radians), with $z_r \neq z_s$, are stored for subsequent use. Secondly, and for each observed dSTEC_o sample, synthetic dSTEC_m values

(in TECU) are computed by

$$\mathrm{dSTEC}_m(t_s) = \mathrm{MF}(z_s)\,\mathrm{VTEC}(\varphi_s, \lambda_s, t_s) - \mathrm{MF}(z_r)\,\mathrm{VTEC}(\varphi_r, \lambda_r, t_r) \tag{10}$$

where φ_r, λ_r and φ_s, λ_s (in degrees) are the coordinates of the corresponding IPPs. Here both $\mathrm{VTEC}(\varphi, \lambda, t)$ are obtained, following Schaer and Feltens (1998), by temporal interpolation between consecutive *rotated* TEC maps

$$\mathrm{VTEC}(\varphi, \lambda, t) = \frac{T_{i+1} - t}{T_{i+1} - T_i}\,\mathrm{VTEC}_i(\varphi, \lambda'_i) + \frac{t - T_i}{T_{i+1} - T_i}\,\mathrm{VTEC}_{i+1}(\varphi, \lambda'_{i+1}) \tag{11}$$

being T_i and T_{i+1} the epochs of the corresponding maps (in hours), with $T_i < t < T_{i+1}$, whereas the rotated longitudes $\lambda'_i = \lambda + 15\,(t - T_i)$ and $\lambda'_{i+1} = \lambda + 15\,(t - T_{i+1})$ compensate the strong correlation between the ionospheric TEC and the (longitude of the) subsolar point. Within each map, the VTEC_i and VTEC_{i+1} are spatially interpolated by a simple 4-point bilinear algorithm (see also Schaer and Feltens, 1998). Finally, the observed minus computed ΔdSTEC (in TECU) are obtained

$$\Delta\,\mathrm{dSTEC}(t_s) = \mathrm{dSTEC}_o(t_s) - \mathrm{dSTEC}_m(t_s). \tag{12}$$

In turn, the RMS of ΔdSTEC, per station, can be computed.

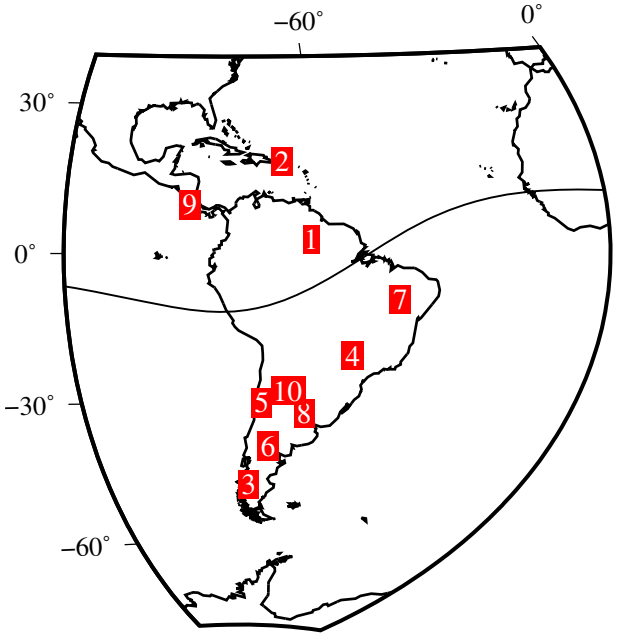

Figure 2: Location of the off-line GNSS stations, listed in Table 4, and employed for the dSTEC evaluation of the near real-time TEC maps. For convenience the geomagnetic equator is also plotted.

In practice, we employed daily RINEX files from ten GNSS stations distributed over the study area (Figure 2). In addition to files from the mentioned data providers we also employed observations from off-line GNSS stations supplied by the Centro Sismológico Nacional (CSN, Chile). The analysis was repeated in four independent days, during the years 2017 and 2018, near the ascending equinox, the descending equinox, the summer solstice and the winter solstice. Also, the TEC maps employed in this analysis are the very same produced for the year-round comparison with the IGS GIMs. However, for these four particular days, additional maps were produced in order to achieve the standard 15 minutes sampling rate of the monitoring system.

In summary, the observed dSTECs are fairly reproduced by the synthetic values, implying that the near real-time maps, in combination with the corresponding mapping function, are capable of representing the regional ionospheric TEC with an average accuracy better than 1 TECU (Table 4). Finally, the three stations leading to a total RMS > 0.7 TECU are located in areas where the IPPs coverage is, systematically, not optimal (especially near BOAV and PUMO, but to a lesser extent also near PISR, see Figure 1 in Mendoza et al., 2019), right). This suggests that the monitoring system could benefit from the use of additional data from GNSS stations located in these specific areas.

Table 4: Per station daily and total RMS (in TECU) resulting from the dSTEC evaluation of the near real-time ionospheric TEC maps.

GNSS Station		2017			2018	Total	ΔdSTEC
#	ID	Jun 21	Sep 22	Dec 21	Mar 20	RMS	Samples
1	BOAV	0.59	1.17	1.01	0.75	0.91	38611
2	BYSP	0.44	0.43	0.32	0.50	0.43	24498
3	CCHR	0.47	0.65	0.84	0.54	0.61	16690
4	ILHA	0.28	0.64	0.89	0.58	0.66	35539
5	JUNT	0.84	0.41	0.42	0.73	0.64	12793
6	MA01	0.26	0.52	0.86	0.46	0.59	23448
7	PISR	0.43	0.80	1.11	0.86	0.84	20104
8	PRNA†	–	0.23	0.62	0.42	0.50	17036
9	PUMO	0.51	0.73	0.51	1.44	0.89	23461
10	TERO	0.30	0.93	0.54	0.65	0.65	39588

†No daily RINEX file, for June 21, 2017, was available.

3 Conclusions and Outlook

A multi-GNSS, operational, high-rate and openly accessible ionospheric TEC monitoring system for South America has been successfully developed, tested and implemented (Mendoza et al., 2019). Both the comparison of the produced maps against global products, including several final IGS GIMs, and also against independent and highly accurate dSTEC observations, resulted in no significant biases nor in unreasonable variances or RMS. On the oder hand, the monitoring system described here could certainly be improved in several ways. For example, the employment of observations at a higher rate could improve the data cleaning stage, resulting in less discarded observations. Data with a higher sampling rate could also open the possibility to reliably repair the cycle-slips, resulting in longer phase-continuous intervals, which in turn could reduce the systematic biases introduced during the carrier-to-code leveling process. Furthermore, the final spatial TEC mapping could be performed in a sun-fixed frame, or it could be parametrized in modified dip latitude instead of geographic latitude, or it could employ a different basis of analytical functions, just to mention some possible improvements. Moreover, while we are actually employing the classical double-frequency approach, to retrieve the ionospheric delay from the GNSS observations, a true triple-frequency methodology (see, e.g., Spits, 2012) could also be considered for those particular stations equipped with modern receivers. Finally, the (rather small) systematic biases found between our TEC maps and the ones produced by several IGS ACs should be addressed, looking at the differences in mathematical representation and parametrization and their impact on the resulting TEC and IFBs estimates. Comparisons with TEC measurements provided by other techniques or satellite missions could certainly help to identify the sources of these differences.

References

Astafyeva, E., Zakharenkova, I., and Förster, M. (2015). Ionospheric response to the 2015 St. Patrick's Day storm: A global multi-instrumental overview. *J. Geophys. Res. Space Physics*, 120(10):9023–9037.

Ciraolo, L., Azpilicueta, F., Brunini, C., Meza, A., and Radicella, S. M. (2007). Calibration errors on experimental slant total electron content (TEC) determined with GPS. *J. Geod.*, 81(2):111–120.

Coster, A., Williams, J., Weatherwax, A., Rideout, W., and Herne, D. (2013). Accuracy of GPS total electron content: GPS receiver bias temperature dependence. *Radio Sci.*, 48(2):190–196.

European GNSS (Galileo) Open Service (2016). Ionospheric Correction Algorithm for Galileo Single Frequency Users. techreport 1.2, European Commission.

Feltens, J. (2007). Development of a new three-dimensional mathematical ionosphere model at European Space Agency/European Space Operations Centre. *Space Weather*, 5(12).

Ghoddousi-Fard, R., Héroux, P., Danskin, D., and Boteler, D. (2011). Developing a GPS TEC mapping service over Canada. *Space Weather*, 9(6).

Gurtner, W. and Estey, L. (2017). RINEX The Receiver Independent Exchange Format Version 3.03, Update 1. techreport, International GNSS Service (IGS).

Haines, G. V. (1985). Spherical Cap Harmonic Analysis. *J. Geophys. Res.*, 90(B3):2583–2591.

Hernández-Pajares, M., Juan, J. M., Sanz, J., Orus, R., Garcia-Rigo, A., Feltens, J., Komjathy, A., Schaer, S. C., and Krankowski, A. (2009). The IGS VTEC maps: a reliable source of ionospheric information since 1998. *J. Geod.*, 83(3):263–275.

Hernández-Pajares, M., Roma-Dollase, D., Krankowski, A., García-Rigo, A., and Orús-Pérez, R. (2017). Methodology and consistency of slant and vertical assessments for ionospheric electron content models. *J. Geod.*, 91(12):1405–1414.

Hernández-Pajares, M., Juan, J., and Sanz, J. (1999). New approaches in global ionospheric determination using ground GPS data. *J. Atmos. Sol. Terr. Phys.*, 61(16):1237–1247.

Klimenko, M., Klimenko, V., Despirak, I., Zakharenkova, I., Kozelov, B., Cherniakov, S., Andreeva, E., Tereshchenko, E., Vesnin, A., Korenkova, N., Gomonov, A., Vasiliev, E., and Ratovsky, K. (2017). Disturbances of the thermosphere-ionosphere-plasmasphere system and auroral electrojet at 30°E longitude during the St. Patrick's Day geomagnetic storm on 17–23 March 2015. *J. Atmos. Sol. Terr. Phys.*

Mannucci, A. J., Wilson, B. D., Yuan, D. N., Ho, C. H., Lindqwister, U. J., and Runge, T. F. (1998). A global mapping technique for GPS-derived ionospheric total electron content measurements. *Radio Sci.*, 33(3):565–582.

Mendoza, L. P. O., Meza, A. M., and Aragón Paz, J. M. (2019). A multi-GNSS, multi-frequency and near real-time ionospheric TEC monitoring system for South America. *Space Weather*. In preparation.

Nischan, T. (2016). GFZRNX - RINEX GNSS Data Conversion and Manipulation Toolbox (Version 1.05). techreport, GeoForschungsZentrum (GFZ), Potsdam, Potsdam. GFZ Data Services.

Orús, R., Cander, L. R., and Hernández-Pajares, M. (2007). Testing regional vertical total electron content maps over Europe during the 1721 January 2005 sudden space weather event. *Radio Sci.*, 42(3).

Orús, R., Hernández-Pajares, M., Juan, J., and Sanz, J. (2005). Improvement of global ionospheric VTEC maps by using kriging interpolation technique. *J. Atmos. Sol. Terr. Phys.*, 67(16):1598–1609.

Ren, X., Zhang, X., Xie, W., Zhang, K., Yuan, Y., and Li, X. (2016). Global Ionospheric Modelling using Multi-GNSS: BeiDou, Galileo, GLONASS and GPS. *Sci. Rep.*, 6:33499.

Rideout, W. and Coster, A. (2006). Automated GPS processing for global total electron content data. *GPS Solutions*, 10:219–228.

Roma-Dollase, D., Hernández-Pajares, M., Krankowski, A., Kotulak, K., Ghoddousi-Fard, R., Yuan, Y., Li, Z., Zhang, H., Shi, C., Wang, C., Feltens, J., Vergados, P., Komjathy, A., Schaer, S., García-Rigo, A., and Gómez-Cama, J. M. (2018). Consistency of seven different GNSS global ionospheric mapping techniques during one solar cycle. *J. Geod.*, 92(6):691–706.

Rülke, A., Agrotis, L., Caissy, M., Habrich, H., Neumaier, P., Söhne, W., and Weber, G. (2014). IGS Real-Time Service - Status And Future Developments. *Geophysical Research Abstracts*, 16(EGU2014-7429-1). EGU General Assembly 2014.

Schaer, S. (1999). *Mapping and Predicting the Earth's Ionosphere Using the Global Positioning System.* phdthesis, Universität Bern, Philosophisch-naturwissenschaftlichen Fakultät.

Schaer, S. and Feltens, J. (1998). IONEX: The IONosphere Map EXchange Format Version 1. techreport, Astronomical Institute, University of Berne, Switzerland and ESA/ESOC, Darmstadt, Germany. September 17, 2015, update to v1.1.

Spits, J. (2012). *Total Electron Content reconstruction using triple frequency GNSS signals.* phdthesis, Université de Liège, Faculty of Sciences, Department of Geography.

Tange, O. (2011). GNU Parallel: The Command-Line Power Tool. *;login: The USENIX Magazine*, 36(1):42–47.

Wang, C., Shi, C., Fan, L., and Zhang, H. (2018). Improved Modeling of Global Ionospheric Total Electron Content Using Prior Information. *Remote Sensing*, 10(1).

Weber, G., Mervart, L., Stuerze, A., Rülke, A., and Stöcker, D. (2016). *BKG Ntrip Client (BNC) Version 2.12*, volume 49 of *Mitteilungen des Bundesamtes für Kartographie und Geodäsie*. Verlag des Bundesamtes für Kartographie und Geodäsie (BKG), Frankfurt am Main.

Wessel, P. and Becker, J. M. (2008). Interpolation using a generalized Greens function for a spherical surface spline in tension. *Geophys. J. Int.*, 174(1):21–28.

Wessel, P., Smith, W. H. F., Scharroo, R., Luis, J., and Wobbe, F. (2013). Generic Mapping Tools: Improved Version Released. *Eos Trans. AGU*, 94(45):409–410.

Wieczorek, M. A. and Meschede, M. (2018). SHTools: Tools for Working with Spherical Harmonics. *Geochem. Geophys. Geosyst.*, 19.